







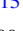





Tidal Interactions between Binary Stars Can Drive Lithium Production in Low-mass Red Giants

Andrew R. Casey^{1,2} , Anna Y. Q. Ho^{3,4} , Melissa Ness^{4,5}, David W. Hogg^{4,6,7,8}, Hans-Walter Rix⁴ , George C. Angelou^{7,9,10} , Saskia Hekker^{11,12} , Christopher A. Tout^{1,13}, John C. Lattanzio¹ , Amanda I. Karakas¹ ,

Tyrone E. Woods^{1,14} , Adrian M. Price-Whelan¹⁵ , and Kevin C. Schlaufman¹⁶ 

¹ School of Physics & Astronomy, Monash University, Clayton 3800, Victoria, Australia; andrew.casey@monash.edu

² Faculty of Information Technology, Monash University, Clayton 3800, Victoria, Australia

³ Cahill Center for Astrophysics, California Institute of Technology, MC 249-17, 1200 E California Blvd, Pasadena, CA 91125, USA

⁴ Max-Planck-Institut für Astronomie, Königstuhl 17, D-69117 Heidelberg, Germany

⁵ Department of Astronomy, Columbia University, 550 W 120th St, New York, NY 10027, USA

⁶ Center for Cosmology and Particle Physics, Department of Physics, New York University, 726 Broadway, New York, NY 10003, USA

⁷ Center for Computational Astrophysics, Flatiron Institute, 162 Fifth Ave, New York, NY 10010, USA

⁸ Center for Data Science, New York University, 60 Fifth Ave, New York, NY 10011, USA

⁹ Max Planck Institut für Sonnensystemforschung, Justus-von-Liebig-Weg 3, D-37077 Göttingen, Germany

¹⁰ Max-Planck Institut für Astrophysik, Karl-Schwarzschild-Str. 1, D-85741 Garching, Germany

¹¹ Max Planck Institute for Solar System Research, SAGE research group, Justus-von-Liebig-Weg 3, D-37077 Göttingen, Germany

¹² Stellar Astrophysics Centre, Dept. of Physics and Astronomy, Aarhus University, Ny Munkegade 120, DK-8000 Aarhus C, Denmark

¹³ Institute of Astronomy, University of Cambridge, Madingley Road, Cambridge CB3 0HA, UK

¹⁴ Institute for Gravitational Wave Astronomy and School of Physics and Astronomy, University of Birmingham, Birmingham, B15 2TT, UK

¹⁵ Department of Astrophysical Sciences, Princeton University, 4 Ivy Lane, Princeton, NJ 08544, USA

¹⁶ Department of Physics and Astronomy, Johns Hopkins University, 3400 N Charles St., Baltimore, MD 21218, USA

Received 2019 February 11; revised 2019 May 23; accepted 2019 June 5; published 2019 August 1

Abstract

Theoretical models of stellar evolution predict that most of the lithium inside a star is destroyed as the star becomes a red giant. However, observations reveal that about 1% of red giants are peculiarly rich in lithium, often exceeding the amount in the interstellar medium or predicted from the big bang. With only about 150 lithium-rich giants discovered in the past four decades, and no distinguishing properties other than lithium enhancement, the origin of lithium-rich giant stars is one of the oldest problems in stellar astrophysics. Here we report the discovery of 2330 low-mass ($1\text{--}3 M_{\odot}$) lithium-rich giant stars, which we argue are consistent with internal lithium production that is driven by tidal spin-up by a binary companion. Our sample reveals that most lithium-rich giants have helium-burning cores ($80^{+7}_{-6}\%$), and that the frequency of lithium-rich giants rises with increasing stellar metallicity. We find that while planet accretion may explain some lithium-rich giants, it cannot account for the majority that have helium-burning cores. We rule out most other proposed explanations for the origin of lithium-rich giants. Our analysis shows that giants remain lithium-rich for only about two million years. A prediction from this lithium depletion timescale is that most lithium-rich giants with a helium-burning core have a binary companion.

Key words: binaries: general – stars: abundances – stars: low-mass

1. Introduction

Stellar evolution theory suggests that material from inner layers, where the element composition has been altered by nuclear reactions, is dredged up to the surface when a star evolves to become a red giant. The surface abundances of certain elements are predicted to change as a consequence of this process. These elements include helium, carbon, nitrogen, and an approximate 95% drop in lithium content (Icko 1967). Observations have repeatedly confirmed these predictions (Lambert & Ries 1981; Gilroy 1989; Kirby et al. 2016), yet also revealed rare examples of otherwise normal giant stars with high surface lithium abundances (e.g., Martell & Shetrone 2013). In some giants the lithium content is higher than what is inferred for the surrounding interstellar medium, indicating that lithium cannot just be preserved: there must be an accretion or production mechanism (Charbonnel & Balachandran 2000). However, the temperature required to produce lithium is also sufficient to destroy it: helium isotopes must be fused together at high temperatures to produce beryllium-7, and beryllium-7 must be transported to cooler regions where lithium can form by electron capture without being immediately destroyed by proton capture (Cameron & Fowler 1971). These

strict requirements make lithium extremely sensitive to the structure and mixing inside a star. Standard theoretical models cannot produce appreciable net amounts of lithium for red giant branch stars. This has prompted several descriptions of non-standard mixing (Sweigart & Mengel 1979; Fekel & Balachandran 1993; Charbonnel 1995; Sackmann & Boothroyd 1999; Charbonnel & Balachandran 2000; Denissenkov & Vandenberg 2003; Lattanzio et al. 2014), as well as hypotheses that lithium production is associated with a specific stage of stellar evolution (Charbonnel & Balachandran 2000; Kumar et al. 2011; Lattanzio et al. 2014), or the result of external phenomena (Andrievsky et al. 1999; Siess & Livio 1999; Denissenkov & Herwig 2004). The lack of evolutionary phase information for a large sample of lithium-rich giants has until now prohibited any empirical constraints on why, where, and when lithium production occurs, and for how long stars remain lithium-rich.

2. Methods

2.1. Spectroscopy

We identified candidate lithium-rich giant stars using public spectra from the LAMOST survey (Data Release 2;

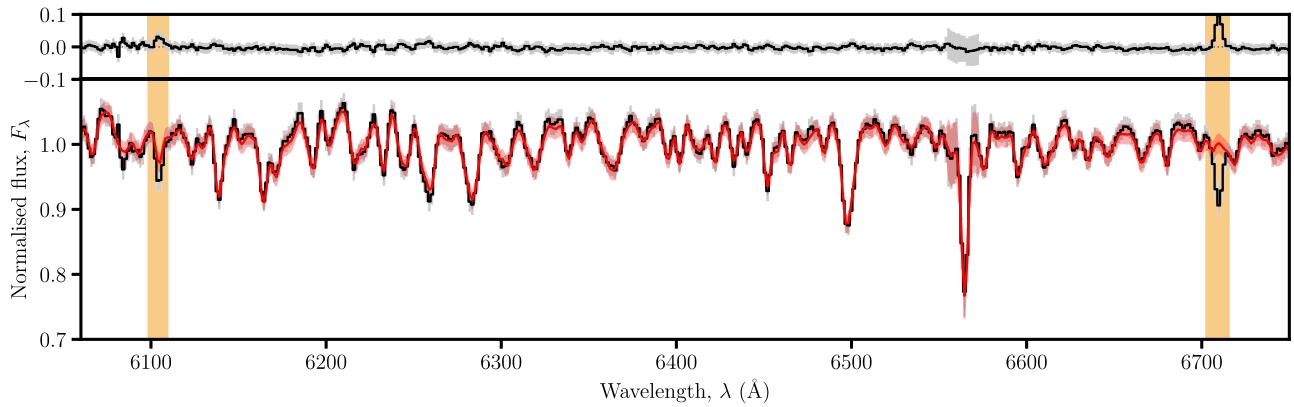


Figure 1. A portion of the LAMOST spectrum and best-fitting model for an example lithium-rich giant star, J055640.1+144534. The data are shown in black and 1σ flux uncertainties are shaded gray. A data-driven model of a lithium-normal star is shown in red, where the quadrature sum of model and data uncertainties are shaded in red. We mark the regions surrounding the 6104 and 6707 Å lithium transitions where we searched for significant residuals.

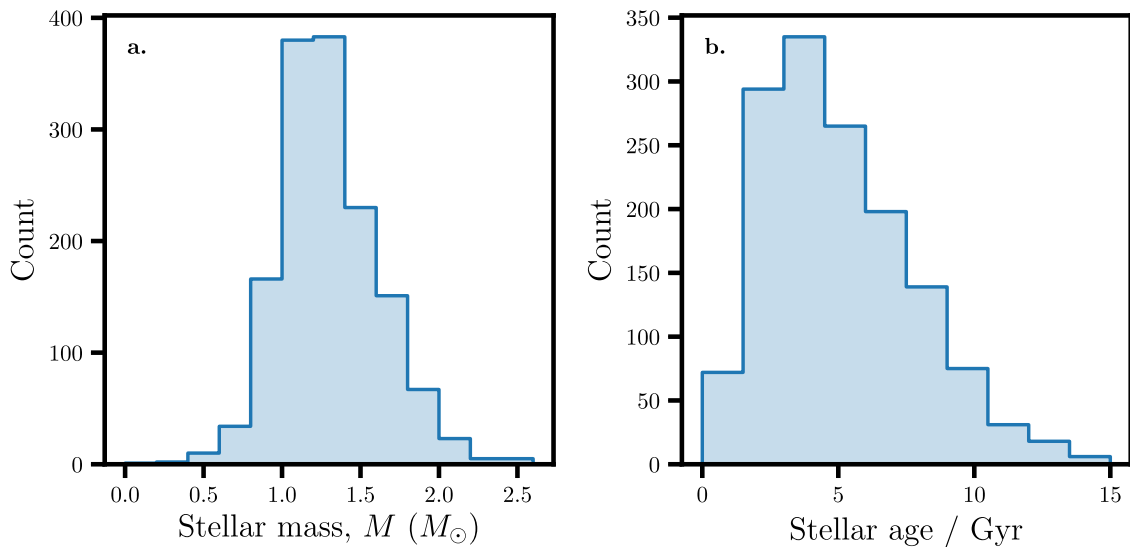


Figure 2. Lithium-rich giants are typically low mass ($1\text{--}3 M_{\odot}$) and show a wide spread in ages. Estimated masses (a) and ages (b) are from $[\text{C}, \text{N}/\text{H}]$ abundance ratios, where the typical estimated uncertainties are $0.25 M_{\odot}$ in mass and 40% in age.

Luo et al. 2015). The LAMOST spectra span from 365 to 900 nm and have a typical resolution of 1800. We searched for significant deviations between the continuum-normalized rest-frame spectrum and a best-fit spectrum from a data-driven model (Figure 1; Ho et al. 2017a, 2017b). We applied a Gaussian matched filter to the residuals between the model and the data at the 6707 Å lithium doublet and the 6104 Å subordinate line. We identified 4558 candidate lithium-rich giants by requiring a 3σ deviation in either region. We visually inspected the spectrum and best-fitting model for every lithium-rich giant star candidate, twice. We discarded any candidate that showed evidence of being a false positive, including spectra with very low signal-to-noise ratios or data reduction issues, as well as any candidate where the lithium deviations were narrower than the expected spectral resolution.

The evolutionary track for low-mass pre-main-sequence stars overlaps with the sub-giant phase in stellar effective temperature and surface gravity (Choi et al. 2016; Dotter 2016). Consequently, we discarded 302 lithium-rich sub-giant candidates because they showed evidence of being young stars,

either through chromospheric activity indicated by emission in $\text{H}\alpha$, or significant photometric variability indicating star spots (McQuillan et al. 2014). We found that most stars with these signatures were spatially concentrated in known young star-forming regions or at low absolute Galactic latitudes.

Using the stellar parameters (T_{eff} , $\log_{10} g$, $[\text{Fe}/\text{H}]$) derived from LAMOST spectra (Ho et al. 2017a), we synthesized the 6707 Å lithium doublet and surrounding region and determined the best-fitting lithium abundance for each star. We used MARCS spherical model photospheres (Gustafsson et al. 2008), the VALD database of transitions (Piskunov et al. 1995), and the *iSpec* (Blanco-Cuaresma et al. 2014) wrapper of the SME synthesis package (Valenti & Piskunov 1996). Using the standard nomenclature of $A(\text{Li}) = \log_{10}(N_{\text{Li}}/N_{\text{H}}) + 12$, where N_X refers to the number density of atoms of a species, we excluded 15 stars with $A(\text{Li}) < 1.5$ as being lithium-normal. We do not apply corrections introduced by the assumption of local thermodynamic equilibrium (LTE) or the use of simplified stellar models; all $A(\text{Li})$ abundances presented here are conditioned on the assumption of LTE and 1D spherical models. The quoted uncertainties on $A(\text{Li})$ are the formal fitting errors conditioned on the stellar parameters.

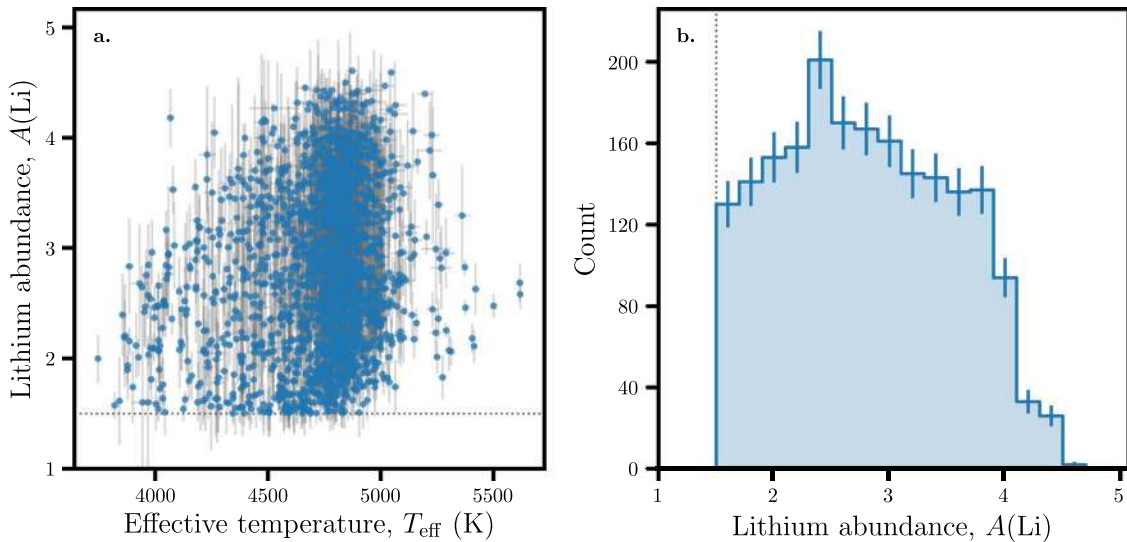


Figure 3. Distribution of measured lithium abundances. (a) Surface lithium abundances against stellar effective temperature for all 2330 lithium-rich giant stars discovered in LAMOST. It is plausible that not all lithium-rich giants with $T_{\text{eff}} > 5000$ K and $A(\text{Li}) = 1.5$ – 2.5 are identified by our matched filter. (b) The distribution of measured lithium abundances. The dotted line in both panels represents the defining limit of $A(\text{Li}) > 1.5$ for a lithium-rich giant star.

These uncertainties are primarily dominated by the signal-to-noise ratio of the LAMOST spectrum, and do not include the uncertainty in stellar parameters. For these reasons, the quoted formal errors may be slightly underestimated.

Our distilled sample contains 2330 lithium-rich giant stars. We show the distribution of $A(\text{Li})$ for these lithium-rich giants in Figure 3. We find that two of our lithium-rich giants are rediscoveries: SDSS J0652+4052 and SDSS J0654+4200 (Martell & Shetrone 2013). The stellar parameters and lithium abundances (T_{eff} , $\log_{10} g$, $[\text{Fe}/\text{H}]$, $A(\text{Li})$) that we derive are all consistent within the joint 2σ uncertainty between this work and the literature, with most measurements agreeing within 1σ of the quoted uncertainty in either study. In particular we find $A(\text{Li}) = 3.47 \pm 0.19$ for SDSS J0654+4200, in good agreement with the previously reported value of $A(\text{Li}) = 3.3 \pm 0.2$, and $A(\text{Li}) = 3.26 \pm 0.08$ for SDSS J0652+4052, 0.04 below the literature value. We also note that LAMOST obtained a high signal-to-noise ratio spectrum for another known lithium-rich giant star (SDSS J0304+3823; Martell & Shetrone 2013), but this was not included in our sample because the residuals surrounding the lithium doublet at 6707 Å reached only 2.7σ , and did not meet our 3σ threshold for detection.

The data-driven model we employed also provides estimates of $[\text{C}/\text{H}]$ and $[\text{N}/\text{H}]$ abundance ratios for all LAMOST spectra. We found that 30 of our lithium-rich ($A(\text{Li}) > 1.5$) giants at the base of the giant branch ($\log_{10}[g(\text{cm s}^{-2})] > 3.2$) have $[\text{C}/\text{N}] > 0$, which indicates that the first dredge-up may not have finished and therefore lithium is not expected to be fully depleted. We include these candidates in our sample but caution that first dredge-up may not have finished and this may explain their high lithium content. We estimated stellar masses and ages from stellar parameters and $[\text{C}, \text{N}/\text{H}]$ abundance ratios for 1374 of our lithium-rich giants, where their stellar parameters and abundance ratios are in the valid range for existing empirical relationships (Martig et al. 2016). These inferred masses indicate that most of our sample are low-mass (1 – $3M_{\odot}$) red giant stars (where the typical uncertainty on mass is $0.25M_{\odot}$), and the distribution of ages peaks at 4.6 Gyr (Figure 2).

2.2. Asteroseismology

Asteroseismology confirms the results we derive from spectroscopy. The evolutionary states for 23 of our lithium-rich giants could be unambiguously determined using high-quality light curves from the *Kepler* space telescope (Figure 4(c); Mosser et al. 2012; Stello et al. 2013; Vrad et al. 2016), which confirms they are low-mass red giant branch stars, and where at least 21 are found to be core-helium-burning stars (perhaps 22; the classification of 1 star is disputed). Another 2 lithium-rich giants have useful light curves obtained during the *Kepler/K2* mission. Our asteroseismic analysis of those *Kepler/K2* light curves reveals that these two upper giant branch stars are first-ascent giants, with likelihood ratios of about 100 when compared to core-helium-burning or asymptotic giant branch phases (Hekker et al. 2017). Ignoring selection effects associated with the *Kepler* and *K2* missions, this asteroseismic sample of 25 suggests that the fraction of lithium-rich giants with helium-burning cores is about $f_{\text{CHeB}} = 0.84$ – 0.88 (21/25–22/25).

We cross-matched the complete LAMOST catalog with a literature source of asteroseismic properties ($\Delta\nu$, $\Delta\Pi_1$; Vrad et al. 2016), which revealed 1365 stars that both have high-quality LAMOST spectra and high-fidelity asteroseismic labels. With these data as a training set, we trained a classifier to estimate $\Delta\Pi_1$ (and other nuisance parameters) given the spectrum of a star. In doing so we identify stars with helium-burning cores as those with an estimated $\Delta\Pi_1 > 150$ s, given the spectrum. Specifically, we modeled the flux in each LAMOST pixel as a second-order quadratic function of the stellar labels (T_{eff} , $\log_{10}[g(\text{cm s}^{-2})]$, $[\text{Fe}/\text{H}]$, $\Delta\nu$, and $\Delta\Pi_1$) and a single noise term per pixel. We performed cross-validation experiments ($N_{\text{trials}} = 10$) where we used a random 80% of the training set as the labeled set and the remaining 20% formed as a validation set. From these experiments we find that our model can identify core-helium-burning stars directly from LAMOST spectra with an accuracy (recall) of 93.4% (precision 96.9%; F -measure 0.95). The astrophysical interpretation here is that individual pixels in the spectrum are weakly informative about

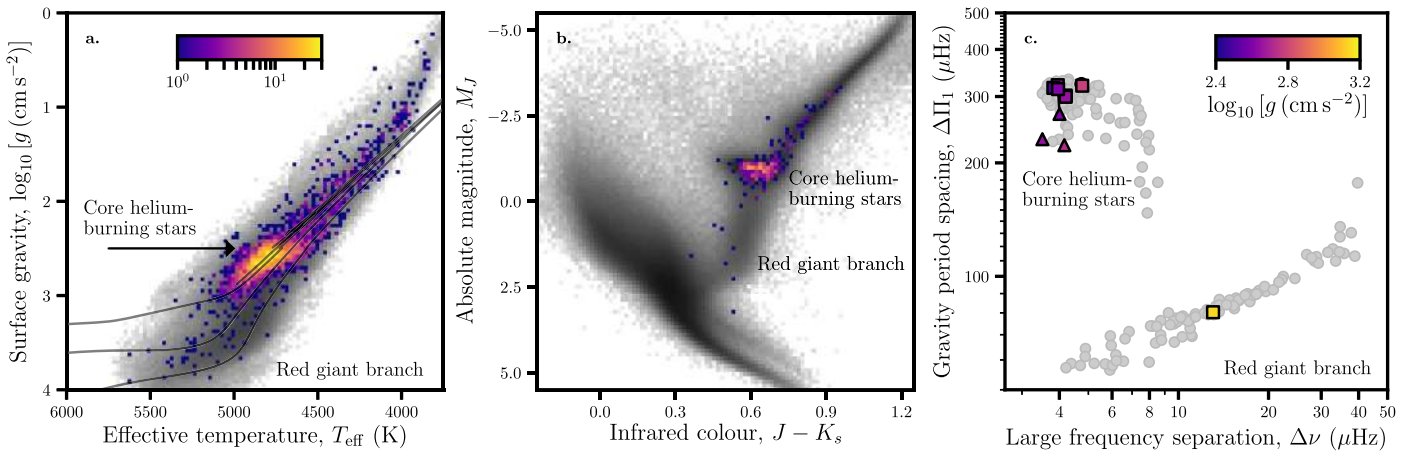


Figure 4. Most lithium-rich giants have helium-burning cores. (a) Stellar parameters for all giants in LAMOST (shown as logarithmic density in gray) and 2330 lithium-rich giants colored by logarithmic density. Overlaid are three representative evolutionary tracks (Choi et al. 2016; Dotter 2016) with $[\text{Fe}/\text{H}] = -0.15$ and $M = 1, 1.5,$ and $2 M_{\odot}$. (b) Infrared color and absolute magnitude for 240 lithium-rich giants with high-quality *Gaia* parallaxes. The density color scale in panel (b) is matched to panel (a). The entire *Gaia*-TGAS sample is shown in gray (Anderson et al. 2018; Gaia Collaboration et al. 2018). (c) Asteroseismic period spacings for lithium-rich giants in the *Kepler* field. Marker shapes (circles (Mosser et al. 2012), squares (Stello et al. 2013) and triangles (Vrard et al. 2016) indicate the literature source. For context, we show the asteroseismic properties of typical giant stars in gray (Mosser et al. 2012). The arrows and markers in a. and b. are indicative only; CHeB stars are identified by a classifier (Section 2.2) when no asteroseismic observables are available.

the $[\text{C}/\text{H}]$ and $[\text{N}/\text{H}]$ abundance ratios, and perhaps the $\text{C}_{12}/\text{C}_{13}$ isotope ratio, which are all expected to be different for red giant branch stars and red clump stars with otherwise almost indistinguishable stellar parameters (e.g., T_{eff} , $\log_{10}[g \text{ (cm s}^{-2}\text{)}]$, $[\text{Fe}/\text{H}]$).

We applied this classifier to all 2330 lithium-rich giants in LAMOST and find that the fraction of lithium-rich giants with helium-burning cores is $f_{\text{CHeB}} = 0.80^{+0.07}_{-0.06}$ (95% confidence interval). This result is only negligibly dependent on the *Kepler* selection function, and is fully consistent with what we find from the small sample of lithium-rich giants with reported asteroseismic properties ($f_{\text{CHeB}} = 0.84\text{--}0.88$). For these reasons, we take the fraction of lithium-rich giants with helium-burning cores to be $f_{\text{CHeB}} = 0.80^{+0.07}_{-0.06}$ for the remainder of this work.

2.3. Timescales

The relative timescales of different stages of stellar evolution are known with high precision, and are not model-dependent. Without yet prescribing a mechanism for lithium enrichment, our sample size allows us to infer when stars become lithium-rich, and how long they remain lithium-rich. We modeled the expected distribution in stellar parameters using evolutionary tracks (Choi et al. 2016; Dotter 2016) for three different scenarios where giants could become lithium-rich:

- at the luminosity bump (e.g., Charbonnel & Balachandran 2000),
- at the tip of the red giant branch (e.g., Lattanzio et al. 2014), or
- either during the core-helium-burning phase or at a random time on the giant branch.

For each lithium-rich giant star we selected the closest evolutionary track in mass and metallicity (Choi et al. 2016; Dotter 2016). Lithium-rich giants without estimated masses were excluded from this analysis, and we used asteroseismic masses where available in preference to masses inferred from carbon and nitrogen abundances. For each tested scenario we assign a point along the selected evolutionary track where the

giant would become lithium-rich, and a time for which it remained lithium-rich. Hereafter, we refer to this timescale as the lithium depletion timescale. By combining the lithium-rich sections of each track, we calculate the normalized distribution of stellar parameters (T_{eff} , $\log_{10} g$) we would expect to observe for lithium-rich giant stars. For example, if stars become lithium-rich at the luminosity bump and only remain lithium-rich for an instant then the expected distribution in $\log_{10} g$ would only show stars close to the luminosity bump. But if stars remain lithium-rich for say 10^8 yr, long enough to evolve beyond the tip of the giant branch, then we would expect lithium-rich giants throughout the upper red giant branch, and some fraction of them to have helium-burning cores. Lithium depletion timescales between 10^4 and 10^8 yr were considered for all scenarios, and in each case we convolved the expected distribution in stellar parameters with the median observational uncertainties.

In scenario (a), lithium production takes place at the luminosity bump on the giant branch. We identify the bump as the first luminosity reversal (brightness decrease) that occurs on the giant branch in the evolutionary track. We find that lithium depletion timescales of at least 10^8 yr are required to produce lithium-rich giants with helium-burning cores in this scenario (Figure 5(a)), simply because this is the typical timescale needed for lithium-rich giants to evolve from the luminosity bump to the core-helium-burning phase. However, any timescale of 10^8 yr (or longer) results in at most only 40% of lithium-rich giants having helium-burning cores, which is half the $80^{+7}_{-6}\%$ we infer (95% confidence interval). This is because the time to evolve from the luminosity bump to the tip of the red giant branch is at least as long as the lifetime of core-helium-burning.

In scenario (b) giants become lithium-rich at the tip of the red giant branch. At this point the star contracts rapidly, shrinking by a factor of 10 in radius in less than 10^4 yr, but taking of order 10^6 yr until the star is fully established in the core-helium-burning stage (i.e., a so-called red clump star). For this reason, lithium depletion timescales of at least 10^6 yr are necessary to account for most lithium-rich giants being stable core-helium-burning stars. With this timescale (or longer),

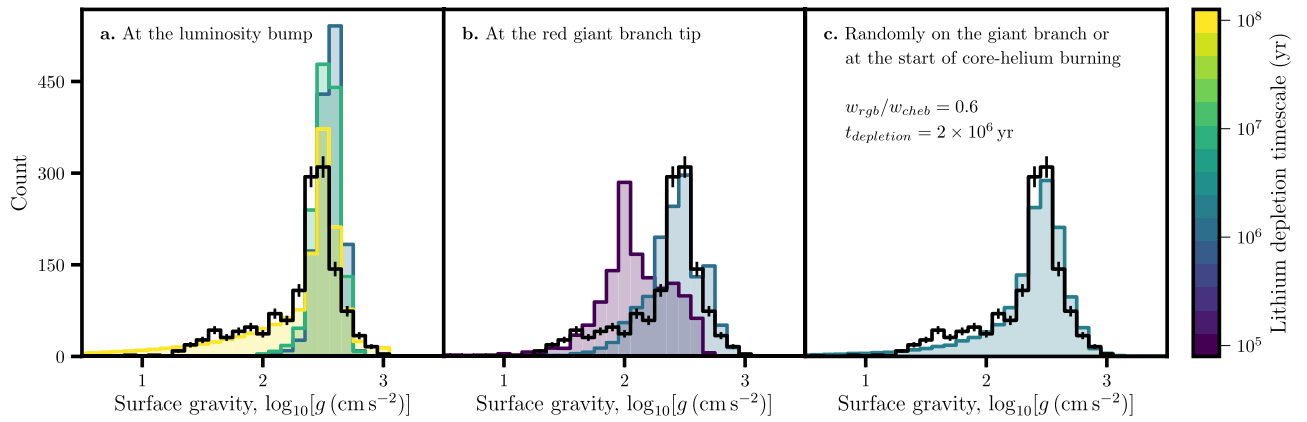


Figure 5. The data are consistent with stars becoming lithium-rich at the start of core-helium-burning, or at a random time on the red giant branch. The observed distribution in $\log_{10}[g(\text{cm s}^{-2})]$ is shown in black (all panels) for 1374 lithium-rich giants with estimated masses, and error bars indicate the relative standard deviation of the number of stars per bin. The expected distribution for lithium production scenarios is shown in each panel. Scenario (a) and (b) cannot produce enough core-helium-burning lithium-rich giants for any depletion timescale: in Scenario (a) at most 40% of lithium-rich giants can have helium-burning cores, which is half the rate we observe $80^{+7}_{-6}\%$. In panel (c) we show the best-fitting lithium depletion timescale from a grid search (see Section 2).

there is a paucity of lithium-rich stars descending from the tip of the giant branch. In fact, *with any timescale*, scenario (b) cannot explain the $20^{+6}_{-7}\%$ of lithium-rich giants that we find to be first-ascendant red giant branch stars, or similar examples known in the literature (e.g., Kirby et al. 2016). If scenario (b) is the predominant mechanism for lithium-rich giants, then another pathway is required to explain first-ascendant red giant branch stars that are lithium-rich.

Scenarios (a) and (b) represent the significant stellar evolution events that occur on the red giant branch. However, no timescale in either scenario provides an adequate explanation for the data. This would indicate that there is not a single phase of stellar evolution where significant internal lithium production occurs. For these reasons we considered a third scenario (c) where stars become lithium-rich at a uniformly random time from just before the luminosity bump until the tip of the giant branch, or they become lithium-rich when they reach the stable core-helium-burning phase. This scenario required us to introduce a relative weighting between the rates of creation of lithium-rich giants at the start of core-helium-burning, relative to those created at some point on the red giant branch. If the lithium depletion timescale were short (i.e., much less than 10^6 yr), then this weighting would exactly reproduce the observed fraction of core-helium-burning stars relative to red giant branch stars. However, when the lithium depletion timescale is longer than the time a star takes to evolve from the red giant branch to the red clump, then some red clump giants we observe may have become lithium-rich on the red giant branch and simply remained lithium-rich until we observe them as red clump stars. To account for the random onset time of lithium production for stars on the giant branch, we made 1000 Monte Carlo draws from a uniform distribution in time for each observed star, where the lower bound is the time of the luminosity bump and the upper bound is the time of the red giant branch tip. In Figure 6 we show the goodness-of-fit χ_r^2 from a grid search of trialed weights and depletion timescales for scenario (c).

If we only consider lithium depletion timescales and weighting fractions that are consistent with our 95% confidence interval of fraction of core-helium-burning stars ($f_{\text{CHeB}} = 0.80^{+0.07}_{-0.06}$), we find that a lithium depletion timescale of about 2×10^6 yr with a relative formation rate of red giant branch stars to core-helium-

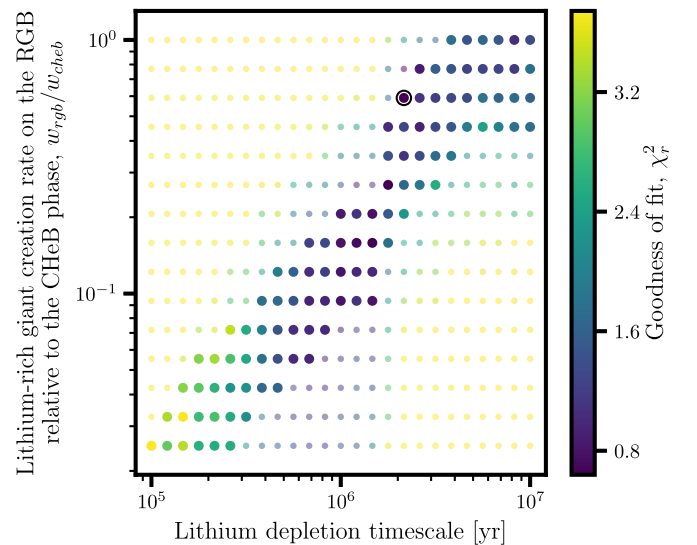


Figure 6. The preferred lithium depletion timescale in scenario (c) is about 10^6 yr. Goodness of fit (reduced χ^2) for a grid search of lithium depletion timescales and weighting ratios. Semi-transparent points indicate that the combination of weight and depletion time predicted core-helium-burning fractions that are outside our 95% confidence interval of $80^{+7}_{-6}\%$, and therefore inconsistent. The preferred model ($w_{\text{rgb}}/w_{\text{chéb}} = 0.6$, $t_{\text{depletion}} = 10^{6.3}$ yr or 2×10^6 yr), with $\chi_r^2 = 0.6$, is marked.

burning stars of 0.6:1.0 ($w_{\text{rgb}}/w_{\text{chéb}} = 0.6$) is preferred with $\chi_r^2 = 0.6$, and provides reasonable agreement with the data (Figure 5(c)). For comparison, χ_r^2 values between 1.9 and 8.4 were found for all timescales considered in scenario (a), and between $\chi_r^2 = 1.5$ and 10 for those in scenario (b). In Section 3 we discuss physical mechanisms that are consistent with scenario (c).

3. Discussion

The main astrophysical parameters for the 2330 lithium-rich giants that we discovered are shown in Figure 4. Our sample size is some 100 times bigger than the largest study to date (Martell & Shetrone 2013). The stellar parameters we derive from spectroscopy suggest that $80^{+7}_{-6}\%$ of lithium-rich giants have helium-burning cores, an analysis that is confirmed through independent expert asteroseismic analyses.

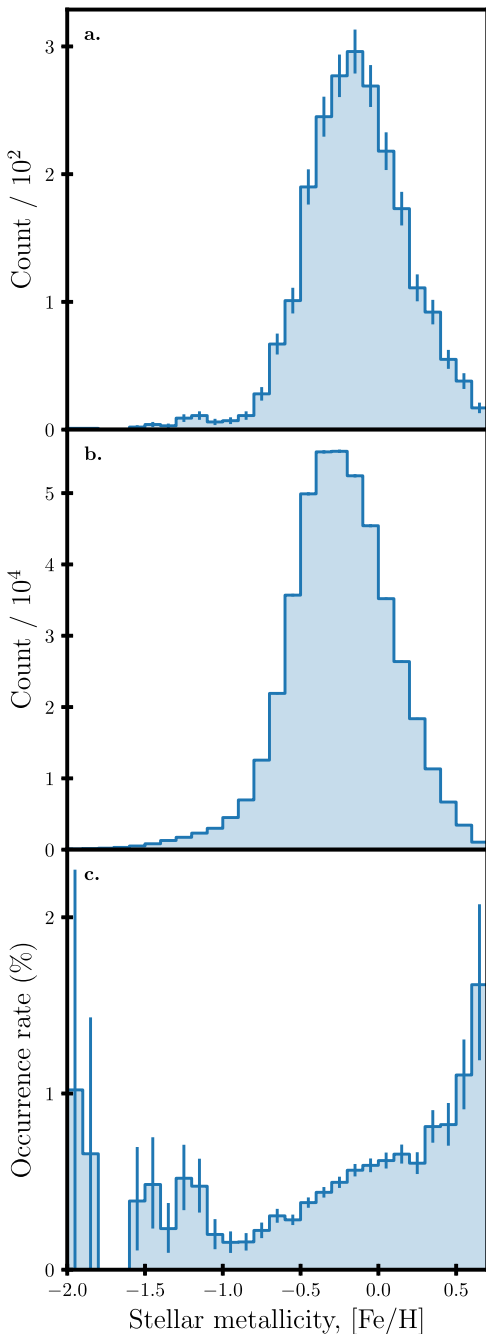


Figure 7. Lithium-rich giants are more frequent at higher metallicities. (a) Metallicity distribution for all 2330 lithium-rich giant stars. The error bars represent the standard deviation of counts per bin. (b) Metallicity distribution for all LAMOST red giants in this sample. (c) The occurrence rate of lithium-rich giants with stellar metallicity. The error bars represent the standard deviation of lithium-rich giants relative to the number of stars per bin.

We find that lithium-rich giant stars occur more frequently with higher stellar metallicity ([Fe/H]; Figure 7). This result reconciles tension between the low frequencies of lithium-rich giants reported in metal-poor environments with well-known completeness statistics (Kirby et al. 2016) (e.g., $0.3\% \pm 0.1\%$ for isolated systems with $[\text{Fe}/\text{H}] \lesssim -0.8$), as compared to field studies of metal-rich stars (Brown et al. 1989) (e.g., 1%–2%). This result has not been observed elsewhere, likely because of the heterogeneous and serendipitous nature of lithium-rich giant star discoveries. Historically, the discovery of a single

lithium-rich giant star has warranted peer-reviewed publication,¹⁷ making it non-trivial to separate any metallicity relationship (or any other observable) from compounding selection effects.

We critically evaluated whether the LAMOST target selection function could make us more or less likely to observe a lithium-rich giant star, and whether the selection function could contribute to the increasing frequency of lithium-rich giants we find with higher stellar metallicity. The LAMOST target selection function is a conglomerate of target selections for many simultaneous surveys. An optimization strategy is employed to maximize the number of fibers allocated to potential targets (from any survey) for a single tiling plate, given physical constraints such as fiber collisions. Given that the true distribution (or frequency) of lithium-rich giant stars is not known, these two facts conspire to prohibit us from directly inverting the LAMOST selection function to understand biases.

Some qualitative statements can be made despite this limitation. There is no other observable property common to all lithium-rich giant stars that makes them clearly distinguishable from lithium-normal stars. While some lithium-rich giants do show excesses in infrared magnitudes, the LAMOST/LEGUE target selection function (Carlin et al. 2012) only makes use of the optical $g - r$ color and an r magnitude color cut that is extended to match target densities for particular locations on the sky. Therefore, there is nothing obvious in the LAMOST selection function that could conceivably bias us toward, or against, selecting lithium-rich giant stars. We also note that comparisons of the LAMOST red giant branch sample with mock catalogs of the Milky Way do not show a significant bias in population properties (Liu et al. 2017).

If we discard selection effects within LAMOST as negligible, then there may still be lithium-rich giant stars that we do not detect due to a weakened $A(\text{Li})$ line at higher effective temperatures. This is shown in Figure 3, which indicates a possible lack of lithium-rich giants with $A(\text{Li}) = 1.5\text{--}2.0$ and about $T_{\text{eff}} > 5000$ K. It is possible that our 3σ detection threshold means that we do not discover all lithium-rich sub-giant stars with $A(\text{Li}) = 1.5\text{--}2.0$, which could imply that we do not detect all sub-giants that have become lithium-rich due to the engulfment of a close-in giant planet (Casey et al. 2016). However, because our timescale modeling begins near the luminosity bump, if a selection effect is present it will not affect our inferences on the lithium depletion timescale.

Given a lithium depletion timescale and an occurrence rate of lithium-rich giants, we can estimate the typical rate at which lithium-rich giants form ($\dot{N}_{\text{formation}} = N_{\text{objects}}/\Delta t_{\text{lifetime}}$). We assume a constant star formation rate of $2 M_{\odot} \text{yr}^{-1}$ and consider stellar masses between $0.1 M_{\odot}$ and $100 M_{\odot}$ when weighting a typical initial mass function (Kroupa 2001) to find a birth rate of giant stars in the Milky Way (the main-sequence turn-off rate). For an evolutionary track (Choi et al. 2016; Dotter 2016) of a $1.3 M_{\odot}$ solar-metallicity star, the mean of our sample, the lifetime between $\log_{10}[g(\text{cm s}^{-2})] = 3.2$, and the end of the core-helium-burning phase is about 250 Myr. Assuming a steady-state system, this implies that the number of giant stars in the Milky Way with $\log_{10}[g(\text{cm s}^{-2})] < 3.2$ is about 7.5×10^7 . Taking a mean fraction of 0.7% lithium-rich

¹⁷ The literature compilation of lithium-rich giants by Casey et al. (2016) shows that 73% of publications announcing the discovery of lithium-rich giant (s) reported only one or two new lithium-rich giants.

giant stars, and the 305,793 giant stars in LAMOST with $\log_{10}[g(\text{cm s}^{-2})] < 3.2$, we estimate that there are about 527,100 lithium-rich giant stars in the Milky Way. Taking 2×10^6 yr as the lithium depletion timescale, this provides us with a formation rate of $\dot{N}_{\text{formation}} = 0.3 \text{ yr}^{-1}$.

This rate excludes merged binary stars (0.01 yr^{-1} ; Andrievsky et al. 1999) and the engulfment of brown dwarfs (Siess & Livio 1999) as the principal explanation for lithium-rich giant stars (Politano et al. 2010; Ivanova et al. 2013). Moreover, brown dwarfs do not form frequently enough to explain the occurrence rate of lithium-rich giants (Cumming et al. 2008). Although intermediate-mass ($3.5 M_{\odot}$ – $5 M_{\odot}$) asymptotic giant branch stars can produce lithium internally and transfer mass to a companion, they are also too rare to explain the number of low-mass lithium-rich giant stars (Karakas & Lugaro 2016). Nearby novae have been tentatively proposed as an explanation for lithium-rich giants (Gratton & D’Antona 1989); however, the novae rate is about two orders of magnitude different than the rate we infer for lithium-rich giant stars: Shafter (2017) found a novae rate of 50 yr^{-1} , of which $\sim 1/4$ are recurrent novae and $\sim 3/4$ have red giant donors (Schaefer et al. 2014). Although it is possible that only a fraction of novae could produce lithium-rich giants, no lithium-rich giants are known to show other abundance signatures that would be expected from classical novae (Melo et al. 2005). In summary, the formation rate we find excludes most external mechanisms proposed to explain the origin of lithium-rich giants.

Only a few proposed mechanisms remain, which are predominantly associated with stages of stellar evolution. However, our timescale analysis reveals that lithium enrichment is not predominantly associated with either the luminosity bump or the tip of the red giant branch (scenarios a and b), the only two significant stellar evolution phases in a red giant star’s evolution. No lithium depletion timescale in either scenario is able to adequately account for the observed distribution in stellar parameters (e.g., $\log_{10}[g(\text{cm s}^{-2})]$), or reproduce the observed fraction of core-helium-burning lithium-rich giant stars. This would suggest that lithium enrichment is not a consequence of single star evolution.

We find that the data are only consistent with scenario (c), where giant stars can become lithium-rich at the core-helium-burning phase or at a random time on the giant branch. While we do find a relative weighting ($w_{\text{rgb}}/w_{\text{cheb}} = 0.6$) and lithium depletion timescale ($2 \times 10^6 \text{ yr}^{-1}$) that can reproduce the observations, we have yet to argue for any lithium enrichment mechanisms that could occur randomly on the giant branch, or at the start of the core-helium-burning phase.

We argue that the mechanisms most consistent with scenario (c) are the accretion of a planet (Siess & Livio 1999), and the tidal spin-up from a binary companion (Fekel & Balachandran 1993). The accretion of a planet provides a reservoir of unburnt lithium and acts as a mechanism to drive extra mixing that enables internal lithium production. A uniformly random time for lithium enrichment along the giant branch suggests an event that occurs at a time that depends on the properties of that system. Given a suitable distribution of exoplanet masses and periods, planet engulfment is a plausible mechanism that could approximate a uniformly random lithium enrichment time on the giant branch. However, planet accretion can only explain lithium-rich giants that do not have helium-burning cores. As a

star evolves up the giant branch it expands in size until it reaches its maximum stellar radius at the tip of the giant branch, before contracting in radius over the next about 10^6 yr as the star becomes a stable core-helium-burning star. Any reasonably close-in planet (within 0.6 au for a $1.3 M_{\odot}$ solar-metallicity star) would have been accreted early on the giant branch (Figure 8). Without introducing significant tidal decay to bring long-period planets close to the host star, planet accretion cannot explain lithium-rich giants with helium-burning cores. In summary, planet accretion can only be responsible for up to about 20% of lithium-rich giant stars.

The primary mechanism we propose for scenario (c) is tidal interactions between binary stars, which can provide a consistent explanation for all lithium-rich giant stars, including those with and without helium-burning cores. Specifically, here we argue that internal lithium production at the start of the core-helium-burning phase is an expected consequence of tidal locking in a binary system, and tidal interactions could spin up a red giant branch star at a near uniformly random time, depending on the properties of the binary system (Figure 8). This mechanism is reliant on the internal production of lithium through the Cameron–Fowler mechanism (Cameron & Fowler 1971), which is mixed to the surface of the giant star. In single star evolution, no net lithium is created without the introduction of extra mixing. Thermohaline mixing, driven by the burning of helium-3 outside the main hydrogen burning shell, can drive sufficient extra mixing after the luminosity bump to replenish some of the lithium lost during first dredge-up. This helium-3 captures an α -particle to produce beryllium-7, which captures an electron to produce lithium-7. Without rapid mixing to move freshly produced lithium-7 to a cooler region, lithium-7 easily captures a proton to form unstable beryllium-8, which then undergoes fission to helium-4. With rapid mixing the overall lithium abundance can increase inside a star: beryllium-7 is moved to a cooler region where electron capture to lithium-7 can occur, but proton capture on lithium-7 does not occur. However, thermohaline mixing is insufficient to enhance lithium above the initial lithium abundance (Lattanzio et al. 2014). We can surmise that at least two conditions are required for lithium production inside red giants: there must be helium-3 available for the ${}^3\text{He}(\alpha, \gamma){}^7\text{Be}$ reaction to occur, and the level of mixing inside a giant must be sufficient for beryllium-7 to be transported to cooler regions so that the ${}^7\text{Be}(\beta^-, \nu){}^7\text{Li}$ reaction can take place.

We propose that differential rotation, enhanced by a binary companion, can induce sufficiently fast mixing to drive significant internal lithium production (Costa et al. 2002). Let us first consider the case of a single star, without a binary companion. Differential rotation is greatest when a star contracts to a core-helium-burning star and the radius decreases by about a factor of 10 or 20 (Despain 1981). We assume the contraction is homologous such that the moment of inertia $I \propto MR^2$ and if we assume that the total angular momentum $J = I\Omega$ is conserved then $J \propto \Omega R^2$. Thus, the spin Ω increases by a factor of 100–400 when core-helium-burning begins. Rotation in centrally condensed stars (Eddington 1929) generally causes perturbations of order Ω^2 such that any rotationally driven mixing can be expected to increase with spin proportional to Ω^2 . Mixing due to rotation can be

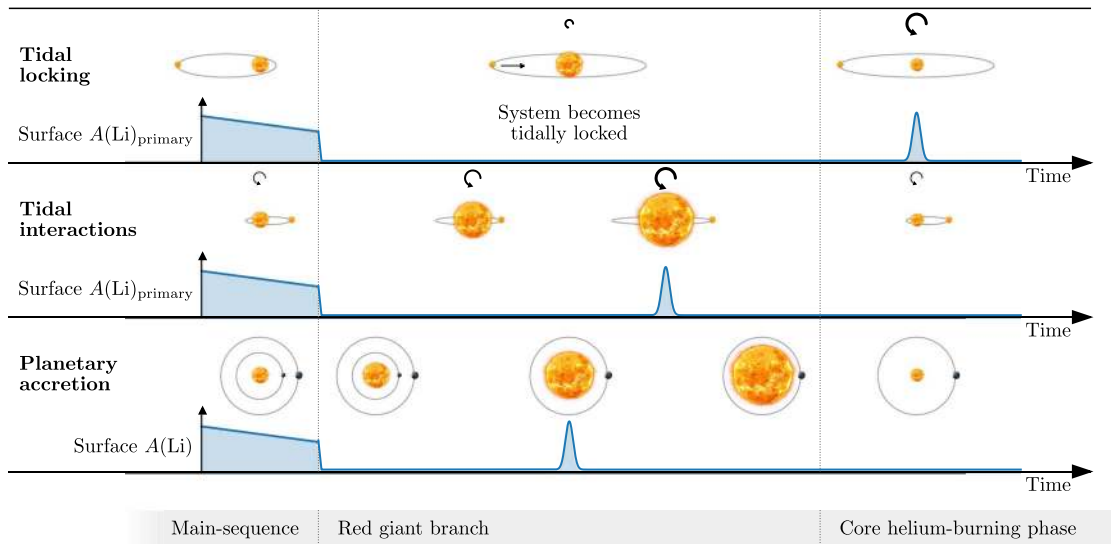


Figure 8. Schematic illustrating the mechanisms that can produce lithium-rich giants at the clump and at a random time on the giant branch. Only tidal locking can produce lithium-rich giants in the core-helium-burning phase. Tidal interactions can spin up the primary when it is on the giant branch (spin is indicated by rotation arrows). Planetary accretion can also cause lithium enrichment (shown in blue) on the giant branch, where the time will depend on the planet’s orbital radius. The schematic is not to scale in length or time.

approximated as a diffusion process with a diffusion coefficient

$$D_{\text{mix}} \approx \frac{L_r r^2}{\mathcal{M}_r g^2} \frac{\nabla_{\text{ad}}}{\nabla_{\text{ad}} - \nabla_{\text{rad}}} \Omega^2 f_i, \quad (1)$$

which rises expectedly with Ω^2 , and it can be shown that $D_{\text{mix}} > 10^{11} \text{ cm}^2 \text{ s}^{-1}$ is necessary to enhance lithium significantly above its initial abundance (Denissenkov & Herwig 2004). However, diffusion coefficients of 10^8 – $10^9 \text{ cm}^2 \text{ s}^{-1}$ are found for normal red giant stars or core-helium-burning stars of similar radii (Denissenkov & Herwig 2004; Palacios et al. 2006), 2–3 orders of magnitude below the $D_{\text{mix}} \approx 10^{11} \text{ cm}^2 \text{ s}^{-1}$ level required for lithium production. In other words, conservation of angular momentum ensures that the rotation of a typical single core-helium-burning star is insufficient to enhance lithium.

A binary companion, however, can provide the additional angular momentum and subsequent higher diffusion coefficient required for lithium production. We used a binary population synthesis code (Hurley et al. 2002) to model the tidal interactions and subsequent spin-up in binary systems. For a representative case of a $1.5 M_{\odot}$ primary star with a $1 M_{\odot}$ companion, the $1.5 M_{\odot}$ primary expands to about $100 R_{\odot}$ on its first ascent of the red giant branch. We require the two stars in the binary system to remain detached, so there is a lower limit to the orbital period such that unstable Roche lobe overflow is avoided.

With a $1 M_{\odot}$ companion the primary fills its Roche lobe in an orbit with a semimajor axis $a = 241 R_{\odot}$, which corresponds to an orbital period of $P_{\text{orb}} = 279$ days. In this binary system configuration the giant primary is tidally locked early in its ascent of the giant branch so that at the point of helium ignition the primary has spin $P_{\text{spin}} = P_{\text{orb}} = 279$ days. After the helium core flash the primary shrinks to a radius of about $10 R_{\odot}$. If we assume the collapse is homologous, then the angular velocity increases as $1/R^2$ or by a factor of about 100. This spins up the primary to $P_{\text{spin}} = 2.14 \times 10^5 \text{ s}$ and an equatorial velocity of 182 km s^{-1} . Because $P_{\text{orb}} = 279$ days is the shortest period this representative binary system configuration can accommodate

while avoiding mass transfer, 182 km s^{-1} corresponds to the maximum spin-up of the primary during the core-helium-burning phase.

As an upper limit to the binary period we require that the tidal synchronization must be sufficient before the primary reaches the tip of the giant branch. We find this requires initial periods about ten times longer than the previously determined minimum orbital period ($P_{\text{orb}} = 279$ days) or $P_{\text{init}} = 7.64$ yr. At larger periods the tides are too weak to have an effect on the spin of the primary. After the helium core flash the primary shrinks and the core-helium-burning star in such a system increases its spin as usual, and it rotates ten times slower than is found for our shortest period configuration. This produces an equatorial velocity of 18 km s^{-1} , which is still fast compared to most giants. For a representative case of a $1.5 M_{\odot}$ primary giant and a $1 M_{\odot}$ companion, 18 and 182 km s^{-1} represent the lower and upper bounds of equatorial velocities expected from the tidal spin up of a companion. This range of tidal spin-up would increase D_{mix} by up to a factor of about 6500 ($D_{\text{mix}} \approx 10^{12}$ – $10^{13} \text{ cm}^2 \text{ s}^{-1}$), orders of magnitude above the requisite value to drive internal lithium production ($D_{\text{mix}} \approx 10^{11} \text{ cm}^2 \text{ s}^{-1}$).

This calculation demonstrates that tidal interactions between binary stars can drive lithium production in low-mass red giant branch stars. If we adopt a normal distribution in $\log[P(\text{days})]$ with a peak at $\log P = 5.03$ and $\sigma_{\log P} = 2.28$ (as inferred from observations; Raghavan et al. 2010), then up to 1 in 3 giants in a binary system could be affected by tidal spin up. The effect of metallicity is to change the maximum radius of the giant (to $71/87/155/175 R_{\odot}$ for $Z = 0.0001/0.001/0.02/0.03$, respectively), while the effect on the radius of the core-helium-burning star is to change by only about 10% over the same range. The range of periods over which stars become tidally synchronized on the red giant branch varies accordingly as $P \propto R^{3/2}$ and the spin up is weaker by R^2 , so the final spin of a tidally synchronized core-helium-burning star scales as $R^{-1/2}$.

Tidal interactions in binary systems would be consistent with an existing link proposed between lithium enrichment and projected surface rotation. Giant stars are generally considered fast rotators if their projected surface rotation, $v \sin i$, exceeds

20 km s⁻¹. The spectral resolution of LAMOST prohibits us from detecting projected surface rotation below 120 km s⁻¹. However, 103 of our lithium-rich giant stars appear in a study of stellar rotation in LAMOST (Frasca et al. 2016). Out of 103 lithium-rich giants, 3 have projected surface rotation significantly above the LAMOST detection limit: between 150 and 260 km s⁻¹. The remaining 100 lithium-rich giant stars have upper limits of less than 120 km s⁻¹. We find that 140 of our lithium-rich giants were observed as part of the APOGEE survey (Abolfathi et al. 2018). Only 5 of those 140 have measurements of $v \sin i$, ranging from 16 to 76 km s⁻¹. We also find 13 stars in common between our sample and the fifth data release of the RAVE survey (Kunder et al. 2017) and 11 of these have $v \sin i$ measurements ranging from 20 and 41 km s⁻¹.

We assume that selection effects in RAVE, LAMOST, and APOGEE have no dependence on $v \sin i$, and that there are no systematic biases in $v \sin i$ between these surveys. We further assume that there are no other phenomena that would contribute to whether or not $v \sin i$ can be measured and infer that, if $v \sin i$ is not reported then $v \sin i$ is so low that it could not be measured. This detection floor is 120 km s⁻¹ for LAMOST (Frasca et al. 2016), about 10 km s⁻¹ for RAVE (Siebert et al. 2011), and about 4 km s⁻¹ for APOGEE (Deshpande et al. 2013). With these assumptions we can naively state that 1.2% (3/256) of lithium-rich giants have $v \sin i$ that exceeds 120 km s⁻¹. For the lithium-rich giants in LAMOST that were also observed by RAVE and APOGEE, we conclude that about 10.5% (16/153) of lithium-rich giants are fast rotators ($v \sin i \gtrsim 20$ km s⁻¹). If the lithium depletion timescale is about 10⁶ yr and the spin-down timescale is about 10⁵ yr (Tout & Pringle 1992), then we can expect about 10% of lithium-rich giants to show some level of enhanced rotation. We assume that the rotational velocities of stars experiencing spin-down are uniformly distributed between spun-up and a representative level of 5 km s⁻¹ for giants that have not experienced tidal interactions. For spun-up giants we take $v \sin i \approx 18$ km s⁻¹ for stars in the widest tidally locked systems and 182 km s⁻¹ for the closest. Given these assumptions the fraction of lithium-rich giants that we expect to have rotation above 120 km s⁻¹ among the entire population (whether they were observed or not), is $f_{>120} = 1 - (150 - 5)/(182 - 5) = 0.18$.

The fraction of lithium-rich giants that we expect to have rotation exceeding 150 km s⁻¹ is given by $f_{\text{observe} > 150} = \frac{t_{\text{spindown}}}{t_{\text{depletion}}} f_{\text{CHeB}} f_{>150}$. Our analysis indicates that about 80% of lithium-rich giants are core-helium-burning giants ($f_{\text{CHeB}} = 0.80$). Given our assumptions we conclude that about 1.5% of lithium-rich giants with helium-burning cores should have surface rotation exceeding 150 km s⁻¹. This is in good agreement with the 1.2% (3/256) we observe from the naive combination of LAMOST, RAVE, and APOGEE data. If we only consider lithium-rich giants with $v \sin i$ measurements from RAVE or APOGEE, then we can repeat this calculation for lower detectable rotational velocities. Taking $f_{>20} = 1 - (20 - 5)/(182 - 5) = 0.92$, we find that 7.4% of lithium-rich giants are expected to have surface rotation exceeding 20 km s⁻¹. This, too, is in reasonable agreement with the 10.6% (16/153) of lithium-rich giants observed to have rotation exceeding 20 km s⁻¹ in the RAVE and APOGEE cross-matches. Given our assumptions, our naive treatment of the combination of multiple catalogs, and our ignorance on the inclination angle, we conclude that the level of projected

surface rotation among lithium-rich giant stars is consistent with tidal spin-up by a binary companion.

We have argued that lithium production driven by tidal interactions is consistent with the observations, but what evidence is there for binarity among lithium-rich giants? Lithium-rich giants are not usually subject to repeat spectroscopic observations, as a single high-quality spectrum is typically sufficient to derive detailed chemical abundances and isotopic ratios, and most literature discussion to date has focused on alternative hypotheses for lithium enrichment. For this reason, almost no lithium-rich giants have been repeatedly observed for radial velocity variations that would indicate binarity. This is largely the case for our sample: most sources have a single epoch in LAMOST and RAVE, or just a few in APOGEE. However, 8 lithium-rich giants were serendipitously discovered by an exoplanet host star survey (Adamów et al. 2015), where multiple epochs of radial velocity measurements are available. Of those lithium-rich giants, 5 out of 8 showed radial velocity variations from just a few epochs, a curiously high fraction given the long orbital periods where tides could drive lithium production. A precise radial velocity study of a large number of lithium-rich giants is well-motivated, but the long orbital periods make such an endeavor expensive.

While tidal interactions between binary stars would provide a consistent explanation for the data, some alternative explanations merit discussion. If planet accretion is responsible for the 20% of lithium-rich giants that are on their first ascent on the giant branch, then the remaining 80% could be explained by some mechanism associated with the core-helium flash that occurs at the tip of the red giant branch. The core-helium flash is a turbulent event, and is extremely challenging to model accurately in stellar evolution. Velocity fluctuations are necessarily suppressed, which limits the inferences one can make on internal mixing and subsequent lithium production. Let us consider that the data are explainable by scenario (c) where the physical mechanisms are planet engulfment and internal lithium production arising from the core-helium flash. If so, why do some stars become lithium-rich during core-helium flash, and some do not? Do tidal interactions have no impact on lithium production, even though mixing is a key ingredient? The answer to these questions is, quite obviously, that we do not know because we cannot accurately model the helium flash. Even without a detailed understanding of the core-helium flash, we know that if the core-helium flash were to drive lithium production, then a reservoir of helium-3 is necessary just outside the main hydrogen burning shell. However, without differential rotation along the giant branch, most helium-3 will be depleted by extra mixing by the time the star reaches the tip of the giant branch (although a small amount will be continually produced by the hydrogen shell). Presumably, the helium-3 reservoir would be provided during the nucleosynthesis and mixing that results from the core-helium flash.

Although it may be challenging to unambiguously show that the core-helium flash is responsible for internal lithium production, our hypothesis does provide a number of falsifiable predictions. If planet accretion is responsible for enhanced lithium in red giants without helium-burning cores, then an increase in beryllium is also expected (Suess & Livio 1999; Melo et al. 2005). If tidal interactions are responsible, then we would expect the long-lasting extra mixing from the spin-up of a binary companion to fully deplete the beryllium in a star

(Sackmann & Boothroyd 1999). Similarly, for planet accretion to explain core, helium-burning, lithium-rich giants, planet engulfment would have to occur when the star is at the tip of the red giant branch, and the star has since evolved into the stable core-helium-burning phase and lithium will deplete within the next $\approx 10^6$ yr. If tidal interactions—and more specifically, tidal locking—are the mechanism for lithium enrichment among core-helium-burning stars, then we predict most core-helium-burning lithium-rich giants to have a binary companion.

4. Conclusions

We report the discovery of 2330 lithium-rich giant stars identified from low-resolution LAMOST spectra, a sample size some 100 times larger than any other to date. We find that lithium-rich giant stars occur more frequently with higher stellar metallicity, a result that reconciles tension between precise estimates of occurrence rates in metal-poor environments, and significantly higher occurrence rate estimates derived from the (metal-rich) field. We find that $80_{-6}^{+7}\%$ of lithium-rich giant stars have helium-burning cores.

We find that lithium-rich giant stars cannot be solely explained by lithium production at the luminosity bump, or at the tip of the red giant branch, suggesting that lithium-rich giants are not a consequence of single star evolution. However, we find that the data are explainable by a scenario where stars either can become lithium-rich at a random time on the giant branch, or at the start of the core-helium-burning phase, and remain lithium-rich for about 2×10^6 yr. Given this lithium depletion timescale and an occurrence rate of lithium-rich giants, we estimate a formation rate of lithium-rich giants of 0.3 yr^{-1} . This formation rate rules out most proposed explanations as the dominant mechanism for lithium enrichment, including stellar mergers, the engulfment of a brown dwarf, mass transfer from an asymptotic giant branch companion, and classical novae.

We argue that a combination of tidal interactions, and possibly planetary engulfment, are the most plausible mechanisms that are consistent with the data. However, because a giant star increases in radius as it ascends the giant branch, planetary engulfment can only explain up to about 20% of lithium-rich giants (e.g., those without helium-burning cores), as any core-helium-burning lithium-rich giant stars will have radii some 10–20 times lower than its radius on the giant branch, and therefore be unable to ingest giant planets without introducing significant tidal decay to bring long-period planets close-in. We conclude that tidal interactions seem to be the most dominant and plausible remaining explanation for lithium-rich giant stars.

We have shown that tidal interactions in binary systems can be strong enough to drive internal mixing high enough such that lithium can be produced through the Cameron–Fowler mechanism. This effect is largest in a binary system where a giant star contracts in radius at the start of the core-helium-burning phase, consistent with our scenario. Those same conservation of angular momentum constraints demonstrate that the requisite level of mixing cannot be achieved by a single star without a binary companion. Although there are observational biases, the expected projected rotational velocities resulting from tidal interactions are consistent with observations.

A prediction of our hypothesis is that nearly every lithium-rich giant star with a helium-burning core has a binary




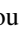





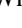
companion, as most of these objects cannot be explained by planet accretion. Similarly, unless the frequency of lithium-rich giants can be explained by an increased planet occurrence rate at higher metallicities, then our hypothesis implies either an increasing binary fraction with increasing stellar metallicity, or that metal-rich stars are more affected by rotation induced by tidal interactions. Distinguishing between tidal spin-up and planet accretion may be possible for individual systems through high-resolution spectroscopic observations to precisely measure beryllium and radial velocity variations. Planetary engulfment is expected to increase both beryllium and lithium (Siess & Livio 1999; Melo et al. 2005), whereas long-lasting extra mixing from the spin-up of a binary companion is expected to fully deplete the beryllium inside a star (Sackmann & Boothroyd 1999).

A. R. C. is supported through an Australian Research Council Discovery Project under grant DP160100637. A. Y. Q. H. is grateful to the community at the MPIA for their support and hospitality during the period in which much of this work was performed. A. Y. Q. H. was supported by a Fulbright grant through the German-American Fulbright Commission and a National Science Foundation Graduate Research Fellowship under grant No. DGE-1144469. M. K. N. and H.-W. R. have received funding for this research from the European Research Council under the European Union’s Seventh Framework Programme (FP 7) ERC grant Agreement No. [321035]. C. A. T. thanks Churchill College for his fellowship and Monash University for hosting him as a Kevin Westfold distinguished visitor. This work was supported by the GROWTH project funded by the National Science Foundation under PIRE grant No. 1545949. The research leading to the presented results has received funding from the European Research Council under the European Community’s Seventh Framework Programme (FP7/2007-2013)/ERC grant agreement (No. 338251, StellarAges). This research has made use of NASA’s Astrophysics Data System. This work has made use of data from the European Space Agency (ESA) mission *Gaia* (<http://www.cosmos.esa.int/gaia>), processed by the *Gaia* Data Processing and Analysis Consortium (DPAC, <http://www.cosmos.esa.int/web/gaia/dpac/consortium>). Funding for the DPAC has been provided by national institutions, in particular the institutions participating in the *Gaia* Multilateral Agreement. Guoshoujing Telescope (the Large Sky Area Multi-Object Fiber Spectroscopic Telescope LAMOST) is a National Major Scientific Project built by the Chinese Academy of Sciences. Funding for the project has been provided by the National Development and Reform Commission. LAMOST is operated and managed by the National Astronomical Observatories, Chinese Academy of Sciences. This paper includes data collected by the *Kepler* mission. Funding for the *Kepler* mission is provided by the NASA Science Mission directorate. This paper includes data collected by the *K2* mission. Funding for the *K2* mission is provided by the NASA Science Mission directorate.

Facilities: LAMOST, *Kepler*, *Gaia*.

Software: *AstroPy* (Astropy Collaboration et al. 2013, 2018), *numpy* (Van Der Walt et al. 2011), *scipy* (Jones et al. 2001), *matplotlib* (Hunter et al. 2007), *The Cannon* (Ness et al. 2015; Casey et al. 2016; Ho et al. 2017a, 2017b).

ORCID iDs

Andrew R. Casey  <https://orcid.org/0000-0003-0174-0564>
 Anna Y. Q. Ho  <https://orcid.org/0000-0002-9017-3567>
 Hans-Walter Rix  <https://orcid.org/0000-0003-4996-9069>
 George C. Angelou  <https://orcid.org/0000-0003-4463-1907>
 Saskia Hekker  <https://orcid.org/0000-0002-1463-726X>
 John C. Lattanzio  <https://orcid.org/0000-0003-2952-859X>
 Amanda I. Karakas  <https://orcid.org/0000-0002-3625-6951>
 Tyrone E. Woods  <https://orcid.org/0000-0003-1428-5775>
 Adrian M. Price-Whelan  <https://orcid.org/0000-0003-0872-7098>
 Kevin C. Schlaufman  <https://orcid.org/0000-0001-5761-6779>

References

- Abolfathi, B., Aguado, D. S., Aguilar, G., et al. 2018, *ApJS*, **235**, 42
 Adamów, M., Niedzielski, A., Villaver, E., et al. 2015, *A&A*, **581**, A94
 Anderson, L., Hogg, D. W., Leistedt, B., Price-Whelan, A. M., & Bovy, J. 2018, *AJ*, **156**, 145
 Andrievsky, S. M., Gorlova, N. I., Klochkova, V. G., Kovtyukh, V. V., & Panchuk, V. E. 1999, *AN*, **320**, 35
 Astropy Collaboration, Price-Whelan, A. M., Sipócz, B. M., et al. 2018, *AJ*, **156**, 123
 Astropy Collaboration, Robitaille, T. P., Tollerud, E. J., et al. 2013, *A&A*, **558**, A33
 Blanco-Cuaresma, S., Soubiran, C., Heiter, U., & Jofré, P. 2014, *A&A*, **569**, A111
 Brown, J. A., Sneden, C., Lambert, D. L., & Edward, J. D. 1989, *ApJS*, **71**, 293
 Cameron, A. G. W., & Fowler, W. A. 1971, *ApJ*, **164**, 111
 Carlin, J. L., Lépine, S., Newberg, H. J., et al. 2012, *RAA*, **12**, 755
 Casey, A. R., Hogg, D. W., Ness, M., et al. 2016, arXiv:1603.03040
 Casey, A. R., Ruchti, G., Masseron, T., et al. 2016, *MNRAS*, **461**, 3336
 Charbonnel, C. 1995, *ApJ*, **453**, 1
 Charbonnel, C., & Balachandran, S. C. 2000, *A&A*, **359**, 563
 Choi, J., Dotter, A., Conroy, C., et al. 2016, *ApJ*, **823**, 102
 Costa, J. M., da Silva, L., do Nascimento, J. D., & Medeiros, J. R. D. 2002, *A&A*, **382**, 1016
 Cumming, A., Butler, R. P., Marcy, G. W., et al. 2008, *PASP*, **120**, 531
 Denissenkov, P. A., & Herwig, F. 2004, *ApJ*, **612**, 1081
 Denissenkov, P. A., & Vandenberg, D. A. 2003, *ApJ*, **598**, 1246
 Deshpande, R., Blake, C. H., Bender, C. F., et al. 2013, *AJ*, **146**, 156
 Despain, K. H. 1981, *ApJ*, **251**, 639
 Dotter, A. 2016, *ApJS*, **222**, 8
 Eddington, A. S. 1929, *MNRAS*, **90**, 54
 Fekel, F. C., & Balachandran, S. 1993, *ApJ*, **403**, 708
 Frasca, A., Molenda-Żakowicz, J., Cat, P. D., et al. 2016, *A&A*, **594**, A39
 Gaia Collaboration, Brown, A. G. A., Vallenari, A., et al. 2018, *A&A*, **616**, A1
 Gilroy, K. K. 1989, *ApJ*, **347**, 835
 Gratton, R. G., & D'Antona, F. 1989, *A&A*, **215**, 66
 Gustafsson, B., Edvardsson, B., Eriksson, K., et al. 2008, *A&A*, **486**, 951
 Hekker, S., Elsworth, Y., Basu, S., & Bellinger, E. 2017, *EPJ Web of Conferences*, **160**, 04006
 Ho, A. Y. Q., Ness, M. K., Hogg, D. W., et al. 2017a, *ApJ*, **836**, 5
 Ho, A. Y. Q., Rix, H.-W., Ness, M. K., et al. 2017b, *ApJ*, **841**, 40
 Hunter, J. D. 2007, *CSE*, **9**, 90
 Hurley, J. R., Tout, C. A., & Pols, O. R. 2002, *MNRAS*, **329**, 897
 Icko, J. I. 1967, *ApJ*, **147**, 624
 Ivanova, N., Justham, S., Nandez, J. L. A., & Lombardi, J. C. 2013, *Sci*, **339**, 433
 Jones, E., Oliphant, T., Peterson, P., et al. 2001, SciPy: Open Source Scientific Tools for Python, <http://www.scipy.org/>
 Karakas, A. I., & Lugaro, M. 2016, *ApJ*, **825**, 26
 Kirby, E. N., Guhathakurta, P., Zhang, A. J., et al. 2016, *ApJ*, **819**, 135
 Kroupa, P. 2001, *MNRAS*, **322**, 231
 Kumar, Y. B., Reddy, B. E., & Lambert, D. L. 2011, *ApJL*, **730**, L12
 Kunder, A., Kordopatis, G., Steinmetz, M., et al. 2017, *AJ*, **153**, 75
 Lambert, D. L., & Ries, L. M. 1981, *ApJ*, **248**, 228
 Lattanzio, J. C., Siess, L., Church, R. P., et al. 2014, *MNRAS*, **446**, 2673
 Liu, C., Xu, Y., Wan, J.-C., et al. 2017, *RAA*, **17**, 096
 Luo, A.-L., Zhao, Y.-H., Zhao, G., et al. 2015, *RAA*, **15**, 1095
 Martell, S. L., & Shetrone, M. D. 2013, *MNRAS*, **430**, 611
 McQuillan, A., Mazeh, T., & Aigrain, S. 2014, *ApJS*, **211**, 24
 Melo, C. H. F., de Laverny, P., Santos, N. C., et al. 2005, *A&A*, **439**, 227
 Mosser, B., Goupil, M. J., Belkacem, K., et al. 2012, *A&A*, **548**, A10
 Ness, M., Hogg, D. W., Rix, H. W., Ho, A. Y. Q., & Zasowski, G. 2015, *ApJ*, **808**, 16
 Palacios, A., Charbonnel, C., Talon, S., & Siess, L. 2006, *A&A*, **453**, 261
 Piskunov, N. E., Kupka, F., Ryabchikova, T. A., Weiss, W. W., & Jeffery, C. S. 1995, *A&AS*, **112**, 525
 Politano, M., van der Sluys, M., Taam, R. E., & Willems, B. 2010, *ApJ*, **720**, 1752
 Raghavan, D., McAlister, H. A., Henry, T. J., et al. 2010, *ApJS*, **190**, 1
 Sackmann, I.-J., & Boothroyd, A. I. 1999, *ApJ*, **510**, 217
 Schaefer, G. H., Brummelaar, T. T., Gies, D. R., et al. 2014, *Natur*, **515**, 234
 Shafter, A. W. 2017, *ApJ*, **834**, 196
 Siebert, A., Williams, M. E. K., Siviero, A., et al. 2011, *AJ*, **141**, 187
 Siess, L., & Livio, M. 1999, *MNRAS*, **308**, 1133
 Stello, D., Huber, D., Bedding, T. R., et al. 2013, *ApJL*, **765**, L41
 Sweigart, A. V., & Mengel, J. G. 1979, *ApJ*, **229**, 624
 Tout, C. A., & Pringle, J. E. 1992, *MNRAS*, **256**, 269
 Valenti, J. A., & Piskunov, N. 1996, *A&AS*, **118**, 595
 Van Der Walt, S., Colbert, S. C., & Varoquaux, G. 2011, *CSE*, **13**, 22
 Vrad, M., Mosser, B., & Samadi, R. 2016, *A&A*, **588**, A87